frontiers in Immunology

TYPE Original Research
PUBLISHED 17 September 2026
DOI 10.3389/fimmu.2026.1872505

Check for updates

OPEN ACCESS

EDITED BY
Marshall Kadin,
University of Virginia, United States

REVIEWED BY
Motohisa Yamamoto,
The University of Tokyo, Japan
Robert Ohgami,
The University of Utah, United States

*CORRESPONDENCE
David C. Fajgenbaum
davidfa@pennmedicine.upenn.edu

RECEIVED 04 May 2026
REVISED 02 July 2026
ACCEPTED 26 August 2026
PUBLISHED 17 September 2026

CITATION
Gonzalez MV, Wang K, Zinski J, Mumau MD, Forsyth KS, Irvine AH, Brandstadter J, Guzman SG, Zhang L, Pierson SK, Austin B and Fajgenbaum DC (2026) Clusterin expression and germinal center morphometry help distinguish idiopathic multicentric castleman disease from select lymphadenopathies. *Front. Immunol.* 17:1872505. doi: 10.3389/fimmu.2026.1872505

COPYRIGHT
© 2026 Gonzalez, Wang, Zinski, Mumau, Forsyth, Irvine, Brandstadter, Guzman, Zhang, Pierson, Austin and Fajgenbaum. This is an open-access article distributed under the terms of the Creative Commons Attribution License (CC BY). The use, distribution or reproduction in other forums is permitted, provided the original author(s) and the copyright owner(s) are credited and that the original publication in this journal is cited, in accordance with accepted academic practice. No use, distribution or reproduction is permitted which does not comply with these terms.

Clusterin expression and germinal center morphometry help distinguish idiopathic multicentric castleman disease from select lymphadenopathies

Michael V. Gonzalez[1], Kaiwen Wang[1], Joseph Zinski[1], Melanie D. Mumau[1], Katherine S. Forsyth[1], Abiola H. Irvine[1], Joshua Brandstadter[2], Stacy G. Guzman[3], Lu Zhang[4], Sheila K. Pierson[1], Bridget Austin[1] and David C. Fajgenbaum[1]*

[1]Center for Cytokine Storm Treatment & Laboratory, Department of Medicine, University of Pennsylvania, Philadelphia, PA, United States, [2]Division of Hematology/Oncology, Department of Medicine, Perelman School of Medicine, University of Pennsylvania, Philadelphia, Pennsylvania, PA, United States, [3]Department of Biochemistry, Biophysics, and Chemical Biology, University of Pennsylvania Perelman School of Medicine, Philadelphia, PA, United States, [4]Department of Hematology, Peking Union Medical College Hospital, Chinese Academy of Medical Sciences and Peking Union Medical College, Beijing, China

Idiopathic multicentric Castleman disease (iMCD) is a heterogeneous cytokine storm disorder involving systemic inflammation, multicentric lymphadenopathy with characteristic histopathology, and life-threatening multiple organ dysfunction. Patients can present with symptoms ranging from thrombocytopenia, anasarca, fever/elevated C-reactive protein (CRP), reticulin myelofibrosis, renal dysfunction, and organomegaly (iMCD-TAFRO) to thrombocytosis, hypergammaglobulinemia, and plasmacytosis (iMCD-IPL), with patients not falling into either group (iMCD-NOS). The molecular mechanisms across the clinical subtypes have not been elucidated and new effective treatments are needed. Here, we performed bulk RNA sequencing and targeted gene expression quantification in lymph node tissue from multiple iMCD clinical subtypes, pathologically related disorders, and controls. We identified 249 upregulated and 42 downregulated genes in iMCD-TAFRO lymph node tissue, which were enriched in the following pathways: angiogenesis, cell proliferation, and various aspects of the humoral and innate immune response. The targeted gene expression analysis revealed shared differentially expressed genes (DEGs) across all three iMCD clinical subtypes, including *SPP1*, *XBP1*, *PRDM1*, and *CLU*. We identified unique DEGs in each iMCD clinical subtype, including *PLA2G2A, MSR1, IL8* (iMCD-TAFRO), *IL9, KIR3DL1, IL18RAP* (iMCD-IPL), and *IL7, TLR8, and CX3CR1* (iMCD-NOS). Since Clusterin (*CLU*) was significantly upregulated in iMCD but not in related conditions, we performed immunohistochemistry and observed that Clusterin is elevated in the germinal center and mantle zone regions of iMCD patient lymph nodes. A composite model incorporating CLU expression in these lymph node compartments with germinal center features demonstrated strong

performance in differentiating iMCD from selected lymphadenopathies. Together, this work identified pathways dysregulated in iMCD lymph nodes and suggests that Clusterin, particularly when integrated with germinal center features, could be a novel biomarker.

KEYWORDS

bioinformatics, Clusterin (CLU), gene expression, idiopathic multicentric Castleman disease (iMCD), lymphadenopathy

Introduction

Idiopathic multicentric Castleman Disease (iMCD) is a rare polyclonal lymphoproliferative disorder of unknown etiology with an annual incidence of approximately 1,500 individuals in the United States and a 25-35% 5-year mortality rate (1–3). iMCD is characterized by a wide range of clinical and pathological features, including multifocal lymphadenopathy with unique histopathologic features and cytokine-driven inflammation (4). Within iMCD, multiple clinical phenotypes exist (5). Patients presenting with thrombocytopenia, anasarca, fever/elevated C-reactive protein (CRP), reticulin myelofibrosis/renal dysfunction, and organomegaly have been defined as iMCD-TAFRO. iMCD with idiopathic plasmacytic lymphadenopathy (iMCD-IPL) is defined by thrombocytosis, hypergammaglobulinemia, and a milder clinical course. Patients who do not meet these clinical criteria are classified as iMCD–not otherwise specified (iMCD-NOS), which has milder clinical features more similar to iMCD-IPL than to iMCD-TAFRO. Patients can also be classified by histopathological subtype, including hyaline vascular/hypervascular, plasmacytic, and a mixed variant that incorporates features of both. However, the clinical implications of these histopathological subtypes remain unclear (6).

The etiology of iMCD is not well understood, and its heterogeneous presentation suggests multiple possible pathophysiological mechanisms. Roughly half of iMCD patients respond to siltuximab, a monoclonal antibody targeting the pro-inflammatory cytokine interleukin-6 (IL-6 (7, 8). Systemic inflammatory symptoms of iMCD can be observed in other inflammatory disorders and hematologic malignancies, complicating its diagnosis. However, gene expression differences in lymph node (LN) tissue between these clinically and pathologically related disorders have not been thoroughly explored, providing fertile ground to better identify more specific features of iMCD.

Most discovery-based investigations of gene expression networks or proteomic signatures involved in iMCD have been done in circulating peripheral blood mononuclear cells (PBMCs) or in plasma/serum, but not in the LN (8–11). Nevertheless, important pathogenic insights have been made. In a large serum proteomics-based study involving 88 iMCD patients and several clinico-pathologically related disorders, we found that the PI3K-AKT-mTOR, angiogenesis, IL-6-JAK-STAT3, and CXCL13 pathways, as well as up-regulated cytokines, were among the most enriched in iMCD serum (3, 8, 9). In PBMCs, we found that interferon-stimulated genes (ISGs) were upregulated and strongly correlated with mTOR signaling in several immune cell types in iMCD patients (10); interestingly, mTOR inhibition is an effective treatment in some patients. More recently, Wing et al. (12) and Horna et al. (13) explored gene expression changes in MCD LN tissue compared to healthy controls. These studies identified plasma cell differentiation (*XBP1*), follicular dendritic cell markers (*CXCL13*, *CLU*), angiogenesis (*VEGF, VEGFR*), mTORC1 pathway genes, and complement cascade signatures that were significantly increased in MCD LN tissues (12, 13). However, the sample size was limited in these studies, and HHV-8 status was not defined in Wing et al. Additionally, subtyping based on the clinical manifestations of MCD was not performed in either study.

Herein, we investigate the LN transcriptome across multiple iMCD subtypes (iMCD-TAFRO, iMCD-IPL, iMCD-NOS) compared to both sentinel controls and clinico-pathologically overlapping autoimmune (systemic lupus erythematosus, SLE) and neoplastic (diffuse large B-cell lymphoma, DLBCL) conditions, and perform targeted studies of genes that distinguish these conditions. Although these subtypes of iMCD have been defined and described (14, 15), the LN transcriptomic differences have not been explored.

Materials and methods

Patient samples and histologic review

Discovery and validation cohorts

We identified samples from 7 patients enrolled in the ACCELERATE natural history registry (NCT02817997) that met criteria for iMCD according to current international diagnostic criteria (16). Additionally, all samples/studies described were approved by the Institutional Review Board of the University of Pennsylvania (IRB # 824758). Based on clinical and laboratory data collected at the time of diagnosis, patients were categorized as iMCD-TAFRO (n=7) (17). Additionally, 7 LN samples resected from breast cancer patients negative for metastasis were chosen to represent controls, herein referred to as sentinel controls (Table 1). Histologically negative sentinel lymph nodes were used as a control group because they represent non-diseased lymphoid tissue obtained through routine clinical care that lack the clinical and pathological features of iMCD and other lymphadenopathies under study. We also obtained LN samples from patients with DLBCL (n=5) from a University of Pennsylvania pathology core service.

In addition to the discovery cohort, we identified 22 additional patients enrolled in the ACCELERATE natural history registry.

10.3389/fimmu.2026.1872505

TABLE 1 Demographic and clinical characteristics of study cohorts.

Characteristic	Discovery: sentinel controls (n=7)	Discovery: iMCD-TAFRO (n=7)	Nanostring: sentinel controls (n=8)	Nanostring: iMCD-TAFRO (n=12*)	Nanostring: iMCD-IPL (n=3)	Nanostring: iMCD-NOS (n=4)	Nanostring: SLE (n=4)	Nanostring: DLBCL (n=5)
Age, mean (SD)	NA	49.1 (12.01)	NA	44.7 (13.71)	40.9 (12.07)	44.4 (16.67)	NA	NA
Sex (M:F)	NA	2:5	NA	4:8	1:2	3:1	NA	NA
Location of tissue sampled, n (%)	NA	Axillary 4 (67%), Groin 1 (16.7%), Mediastinal 1 (16.7%), Not specified 1 (16.7%)	NA	Axillary 5 (41.7%), Inguinal 2 (16.7%), Cervical 1 (8.3%), Groin 1 (8.3%), Mediastinal 1 (8.3%)	Cervical 2 (66%), Groin 1 (33%)	Axillary 2 (50%), Abdominal 1 (25%), Cervical 1 (25%)	NA	NA
Hyaline vascular, n (%)	NA	5 (83.3%)	NA	9 (75%)	1 (33%)	2 (50%)	NA	NA
Plasmacytic or mixed, n (%)	NA	1 (16.7%)	NA	3 (25%)	2 (66%)	2 (50%)	NA	NA
Not specified histology, n (%)	NA	1 (16.7%)						

NA, Not Available; SD, Standard Deviation. *7 iMCD-TAFRO samples in the Nanostring cohort overlap bulk RNAseq samples described in the Discovery cohort.

These patients were categorized into two subtype groups in the validation cohort: iMCD-TAFRO (n=15) and iMCD-NOS/IPL (n=12). The NOS/IPL subtypes were combined because the number of IPL samples was insufficient for comparison (n=1). We also included previously published iMCD samples and sentinel controls (15), which included 8 non-specific MCD and 19 sentinel controls. The composition of the validation cohort is summarized in Supplementary Table 1.

Targeted gene expression cohort

Finally, our targeted gene expression cohort included multiple iMCD clinical subtypes and inflammatory disease comparators. Based on clinical and laboratory data collected at the time of diagnosis, patients were categorized into one of three subtypes: iMCD-TAFRO (n=12), iMCD-IPL (n=3), or iMCD-NOS (n=4) (18). In addition to the iMCD subtype samples, SLE (n=3) and DLBCL (n=5) samples were used as disease comparator groups (Table 1). RNA integrity values were used to select high-quality RNA samples. Samples that overlap between the Discovery and Targeted Gene Expression Cohort can be found in Supplementary Table 2.

Sample preparation and gene expression quantification

RNA extraction from FFPE unstained slides

RNA was isolated from Formalin Fixed Paraffin Embedded (FFPE) tissue sections fixed on slides using the RNeasy DSP FFPE kit (Qiagen, Hilden, Germany). Briefly, sections 10 microns thick were scraped from 5 slides of each sample and submerged in Deparaffinization Solution (DSP) according to the protocol. During this process, tissue digestion using Proteinase K was also done. DNAseI-treated RNA was subsequently isolated using Qiagen's proprietary spin column method, as per the protocol. RNA integrity was assessed using the TapeStation RNA ScreenTape (Agilent, Santa Clara, CA), and concentration was determined using the Qubit 2.0 Fluorometer (Thermo Fisher Scientific, Waltham, MA). Since FFPE RNA is expected to be highly degraded, a DV200 value, representing the percentage of RNA fragments greater than 200 bp, was determined for each sample. In the validation cohort, RNA sample preparation and short-read sequencing were performed as previously described (19).

Preparation of bulk RNA sequencing samples

Libraries for whole transcriptome RNA sequencing were prepared using the Stranded Total RNAseq with Ribo-zero Plus kit (Illumina, San Diego, CA) as per the manufacturer's instructions, starting with an input of 100ng of RNA and 15 cycles of final PCR amplification. Library size was assessed using the 2100 Bioanalyzer and the High-Sensitivity DNA assay (Agilent, Santa Clara, CA). Concentration was determined using the Qubit Fluorometer 2.0. Next-generation sequencing with a paired-end 2x100 bp run length was performed on the NextSeq 2000 platform (Illumina, San Diego, CA). A minimum of 30M reads per sample was acquired for each sample.

Preparation of Nanostring nCounter samples

100 ng of RNA fragments 200 bp and over were used for the NanoString nCounter assay (NanoString, Seattle, WA). Briefly, RNA was hybridized at 65 °C for 19 hours with proprietary fluorescently labeled reporter and capture probes to bind target genes. The hybridized mix of probes and target genes was washed, enriched, and isolated using the NanoString Prep station, and then scanned for fluorescent intensity using the NanoString Digital Analyzer. The nCounter Immunology panel (v2, Supplementary Table 3) was used to quantify 594 genes known to be involved in autoimmune/immune responses, along with 15 internal reference control genes to facilitate normalization.

Informatic and gene expression analysis

Bulk RNAseq analysis in discovery and validation cohorts

RNA-seq reads were demultiplexed using bcl2fastq (Illumina, San Diego). Demultiplexed FASTQ files were aligned to GRCh38 using the Kallisto pseudo-aligner (20) using default settings. The generated BAM files were read into the R statistical computing environment, and gene counts were quantified using the GenomicAlignments package (21). Preliminary QC and differential expression analysis were performed using the R/Bioconductor package DESeq2 (22). Read counts were filtered to include only genes with a read count >=20 in greater than 33% of samples. In the discovery cohort, patients were grouped by phenotype (iMCD-TAFRO, iMCD-NOS/IPL, DLBCL, and sentinel control), and DEGs were considered for further investigation using a $\log_2$ fold change ($\log_2$FC)>|1| and a Benjamini-Hochberg corrected *P*-value<0.05. Gene Set Enrichment analysis (23) (GSEA, v.4.3.2) was performed for the iMCD-TAFRO (n=7) vs. sentinel controls (n=7) discovery cohort using phenotype permutation settings. Gene sets were considered significant if the false discovery rate q-value < 0.25. The Hallmark gene sets from msigDB were used for analysis (24).

For validation, we utilized an expanded cohort comprising data from three sources, as described above. Batch correction was applied to the cohort's normalized expression matrix using the limma package (25). The iMCD-TAFRO and sentinel control samples used in the discovery cohort analysis were removed to maintain independence between datasets. DEG analysis was performed using the same workflow and constraints as the discovery cohort.

Nanostring RNA nCounter assay

Reporter code counts (RCC) were read into R using NanostringQCPro (26). Quality control and normalization were performed using RUVSeq (27, 28). RUVSeq utilizes a panel of 15 housekeeping genes and is able to normalize based on their expression levels (*EEF1G, TUBB, TBP, POLR2A, GUSB, HPRT1, GAPDH, SDHA, OAZ1, PPIA, G6PD, RPL19, POLR1B, ABCF1, and ALAS1*). After normalization, DESeq2 was used to perform differential expression analysis, and DEGs were identified using the discovery cohort criteria.

Estimation and comparison of cell type composition in bulk RNAseq data

Single-cell RNA sequencing data from mesenteric and lung-draining LN tissue from 12 deceased organ donors were downloaded from the CellTypist Immune Atlas (Celltypist.org, accessed June 30, 2023 (29). Annotated cells organized into 13 cell types (B cells, Cycling cells, Dendritic cells, Erythroid, HSC/MPP, ILC, Macrophages, Mast cells, Monocytes, Plasma cells, Promyelocytes, T cells, pDCs) were used to deconvolute the iMCD bulk RNA sequencing samples into estimated cell type proportions using the R-based software tool, Bisque, using a non-negative least-squares regression model (30). Inferred cell proportions per cell type were used to perform composition-based comparisons between iMCD-TAFRO, iMCD-NOS/IPL, and sentinel control samples using a Wilcoxon rank sum test. A Bonferroni correction was used to account for multiple comparisons.

Querying LINCS1000 database to predict drug perturbation efficacy in iMCD TAFRO

L2S2 was used to predict potential reversing therapeutic perturbations (31). The top DEGs from the iMCD-TAFRO versus sentinel control LN comparison (± $\log_2$FC>1.5, adjusted-P < 0.05) were used to construct a gene signature for database entry, and standard settings were used to predict reversing drug perturbations. Predicted reversing drugs were grouped by mechanism of action (MOA) and were ranked by the number of significant individual drugs within that group. For each compound within each cell line, replicate P-values were collapsed into a single line-level value using the MODZ-style robust z-mean (p→z, Tukey biweight mean, z→p) previously employed (32). Line-level P-values for the same compound were then meta-analyzed across cell lines using Stouffer's Z (equal weights), restricting to cell lines with P<0.05 to focus on lines showing significant reversal signal. Scores are reported as $-\log_{10}$P and used for ranking. We repeated the procedure after mapping compounds to MOA to obtain MOA-level scores. Results are presented in four contexts: all lines ("iMCD"), all lines restricted to immune cell lines only ("iMCD-Immune"), iMCD-TAFRO, and iMCD-TAFRO restricted to immune cell lines only (TAFRO-immune). Figures display the top hits by –log10P.

Quantification of follicular clusterin expression and germinal center features for ROC-based discrimination of iMCD from non-CD controls

To label Clusterin in LNs, we immunohistochemically stained for Clusterin using DAB (3,3′-diaminobenzidine) with a hematoxylin counterstain to mark nuclei. Samples overlapping between the previously described discovery and targeted NanoString cohorts and the IHC cohort are listed in Supplementary Table 2. We then identified a DAB threshold to divide Clusterin into positive and

negative regions. To analyze the Clusterin DAB and nuclear hematoxylin stains, we developed a Python-based algorithm quantify Clusterin staining intensity. We used the rgb2hed function from the Python scikit-image library to separate the DAB and hematoxylin channels. We quantified DAB stain in optical density (OD) units. We identified the LN from the background using a global Otsu threshold applied to the LN on the hematoxylin channel. This LN segmentation was used to measure the total LN area. Germinal centers (GCs) and mantle zones (MZs) were manually segmented to attain representative samples. GC, MZ, and interfollicular (IF) regions were manually segmented using the hematoxylin channel alone to blind users to the Clusterin stain. For each sample, the total number of GCs was manually enumerated, using serial H&E sections as a reference for morphological features. We then used the total GC count to randomly identify 10 GCs and MZs for segmentation. To determine statistical significance for all plots, an ANOVA analysis was performed, followed by Tukey tests to compare all conditions. Compartment-resolved Clusterin intensity (IF, MZ, and GC), GC density, and mean GC size were integrated into a model to differentiate between iMCD (n = 20) and non-Castleman nodes (sentinel, SLE, DLBCL, and FDC sarcoma; n = 36) by ROC analysis (scikit-learn) by an L2-regularized logistic-regression model evaluated by repeated stratified 5-fold cross-validation with a nested bootstrap 95% CI and label-permutation significance. Because DLBCL and FDC sarcoma lack mantle zones and germinal centers, those features were set to zero for those cases.

Results

iMCD-TAFRO shows a distinct LN transcriptome profile compared to sentinel controls

Prior to investigating transcriptomic changes in iMCD, we compared DEGs between DLBCL (n=5) and sentinel control LN samples (n=7) with gene expression quantification from a DLBCL cohort of 414 individuals (33). Importantly, we observed several well-established DLBCL gene signatures in our cohort, including minichromosome maintenance complex genes (*MCM2, MCM3, MCM4*), collagen proteins (*COL8A1, COL9A2*), cytokine-mediated signaling and inflammatory genes (*CXCL9, CXCL10*), and interleukins and interleukin receptors (*IL17RB, IL1R2, IL21R, ILDR2*) (Supplementary Table 4**).** The concordance between the DEGs identified in this cohort and published DLBCL literature supports the use of this assay to uncover established transcriptomic changes and explore novel aspects of iMCD biology.

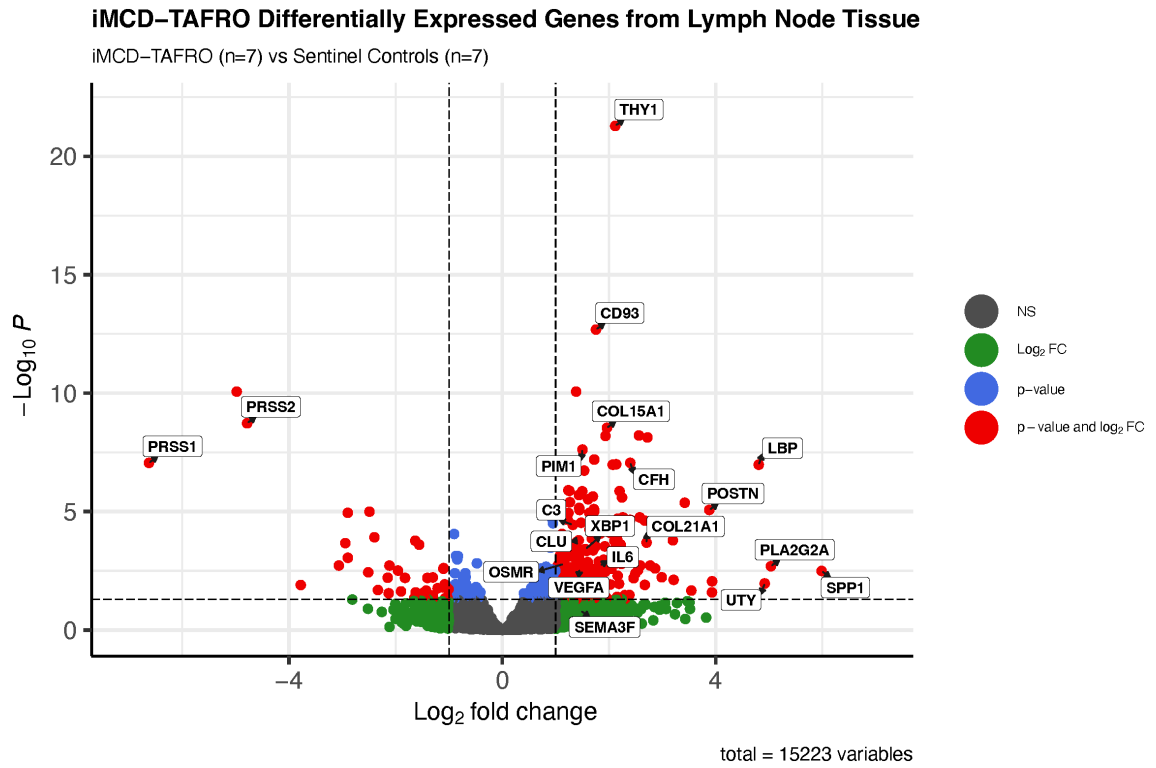


FIGURE 1
Differentially expressed genes in iMCD-TAFRO (n=7) vs sentinel control (n=7) lymph node tissue. A volcano plot of up- and down-regulated genes in iMCD-TAFRO vs sentinel control samples in the discovery cohort. Genes previously implicated in Castleman Disease have been labeled. Vertical dotted lines indicate a +/- log2 fold change (log2FC) threshold of 1, and horizontal dotted lines indicate a threshold for an adjusted P <0.05. Red circles indicate genes that pass both log2FC and adjusted P-value thresholds. Green circles indicate genes that pass the log2FC threshold, but do not have a significant adjusted P-value. Blue circles indicate genes that do not pass the log2FC threshold but have a significant adj. P-value. Grey circles are genes that do not pass either the log2FC or the adj. P-value thresholds.

Next, we applied our approach to iMCD-TAFRO, a homogeneous, phenotypically severe subtype of iMCD that has not been specifically characterized at the transcriptomic level. We performed bulk RNA sequencing on FFPE LN tissue from iMCD-TAFRO patients (n=7) and sentinel controls (n=7). Principal component analysis of the top 500 most variable genes revealed moderate separation between the two groups (Supplementary Figure 1), with PC1 and PC2—enriched with immune-related and cell signaling genes (Supplementary Figures 2A, B)—providing the clearest distinction between iMCD-TAFRO and sentinel control samples.

Differential expression analysis identified 249 genes significantly upregulated in iMCD-TAFRO compared to sentinel controls, and 42 genes were significantly downregulated. The three most up-regulated genes in iMCD-TAFRO were *SPP1*, a multifunctional gene with critical roles in lymphocyte chemotaxis and cytokine regulation, *PLA2G2A*, which is secreted by activated macrophages and platelets and can amplify inflammation, and *UTY*, thought to be involved in chromatin regulation and protein-protein interactions. *IL-6*, a driver of disease progression in some patients, was upregulated and showed a statistically significant increase ($log_2FC=1.83$, adjusted-P = 0.002). Other notable upregulated genes included *CLU*, *THY1, CD93, LBP*, and *SERPINE1*, which are involved in diverse immune responses. Additionally, *POSTN, COL15A1, and COL21A1* contribute to tissue remodeling (Figure 1, Supplementary Table 5).

We then performed gene set enrichment analyses to identify potential gene pathways involved in iMCD-TAFRO pathogenesis

TABLE 2 Significantly enriched hallmark gene pathways in the transcriptome of iMCD-TAFRO lymph node (FDR <0.1, NES >1.5).

Description	Set size	NES	Adjusted p	FDR
EPITHELIAL_MESENCHYMAL_TRANSITION	179	2.98	6.25E-10	1.32E-10
COAGULATION*	98	2.75	6.25E-10	1.32E-10
ANGIOGENESIS	27	2.75	6.25E-10	1.32E-10
TNFA_SIGNALING_VIA_NFKB	183	2.66	6.25E-10	1.32E-10
MYC_TARGETS_V1	192	2.52	6.25E-10	1.32E-10
HYPOXIA	169	2.50	6.25E-10	1.32E-10
MTORC1_SIGNALING	190	2.45	6.25E-10	1.32E-10
INFLAMMATORY_RESPONSE	173	2.40	6.25E-10	1.32E-10
UNFOLDED_PROTEIN_RESPONSE	100	2.37	4.41E-09	9.29E-10
UV_RESPONSE_DN	138	2.26	4.41E-09	9.29E-10
APOPTOSIS*	147	2.20	4.41E-09	9.29E-10
ANDROGEN_RESPONSE	90	2.32	7.72E-09	1.63E-09
IL2_STAT5_SIGNALING	185	2.06	5.86E-08	1.23E-08
COMPLEMENT*	175	2.07	9.47E-08	1.99E-08
INTERFERON_GAMMA_RESPONSE	188	2.02	1.93E-07	4.06E-08
IL6_JAK_STAT3_SIGNALING	76	2.26	2.94E-07	6.19E-08
PROTEIN_SECRETION	91	2.19	3.80E-07	8.01E-08
KRAS_SIGNALING_UP	167	2.01	3.80E-07	8.01E-08
GLYCOLYSIS	171	1.98	5.37E-07	1.13E-07
OXIDATIVE_PHOSPHORYLATION	180	1.98	7.14E-07	1.50E-07
APICAL_JUNCTION	165	1.99	9.43E-07	1.99E-07
G2M_CHECKPOINT	184	1.91	1.88E-06	3.97E-07
ESTROGEN_RESPONSE_EARLY	172	1.93	2.61E-06	5.49E-07
CHOLESTEROL_HOMEOSTASIS*	66	2.02	2.70E-05	5.69E-06
MITOTIC_SPINDLE	195	1.80	4.69E-05	9.87E-06
ESTROGEN_RESPONSE_LATE	161	1.80	4.69E-05	9.87E-06
UV_RESPONSE_UP	134	1.86	8.66E-05	1.82E-05
ADIPOGENESIS	182	1.68	5.40E-04	1.14E-04
TGF_BETA_SIGNALING	53	1.92	5.83E-04	1.23E-04
E2F_TARGETS	190	1.64	6.21E-04	1.31E-04
P53_PATHWAY	176	1.62	1.66E-03	3.49E-04
HEDGEHOG_SIGNALING	30	1.90	1.75E-03	3.69E-04
MYOGENESIS*	148	1.64	1.75E-03	3.69E-04

*Hallmark gene pathways that include CLU.

using the hallmark gene sets from mSigDB (24). 33 out of the 50 hallmark gene sets were significantly enriched in iMCD-TAFRO (Normalized enrichment score, NES>1.5, and FDR q-val<0.05), including pathways involved in immune signaling (e.g., *IL2-STAT5* signaling, *IL6-JAK-STAT3* signaling, *mTORC1* signaling), cellular remodeling (e.g., epithelial-mesenchymal transition, *MYC* targets, angiogenesis), and metabolic reprogramming pathways (e.g., oxidative phosphorylation, glycolysis) (Table 2). Several of these pathways, including angiogenesis and cellular proliferation, have been previously implicated in the pathogenesis of iMCD-TAFRO.

Upregulated transcriptomic changes validated in an independent iMCD-TAFRO cohort

To validate these findings, we performed transcriptomic analyses on an independent cohort of iMCD-TAFRO (n=15) and sentinel control samples (n=19), which were batch-corrected and normalized (Supplementary Figure 3). Of the 249 genes upregulated in the discovery cohort, 220 (88%) were also significantly upregulated in the validation cohort. The remaining 29 genes showed a similar directional trend but did not reach statistical significance. Consistent with this, the 20 most up-regulated genes in the discovery cohort retained their rank order and showed concordant gene expression changes in the validation cohort (Table 3, Supplementary Table 5). We also examined all 15,223 overlapping genes between the two analyses and observed strong concordance across the two datasets; 13,169 (86.5%) exhibited the same direction of change in both DEG analyses (Supplementary Figure 4**;** Pearson correlation coefficient of 0.86, $p<2.2\times10^{-16}$). Together, these results validate the findings in our discovery cohort.

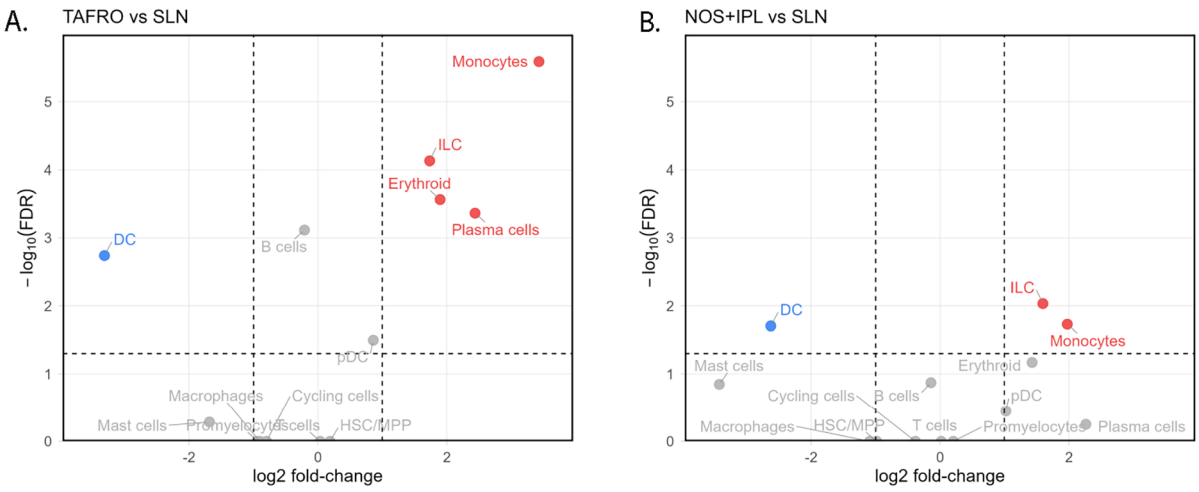
Transcriptomic signatures reveal differential cell type enrichment and potential repurposed treatments

After validating the transcriptomic changes across independent cohorts, we evaluated gene expression in the omnibus bulk RNA-seq cohort (iMCD=37, Sentinel controls=26) across the clinically defined subtypes (iMCD-TAFRO=23, iMCD-IPL/NOS=14) to infer changes in cell type proportions and make treatment predictions. We performed cell type deconvolution to estimate cell type proportions from normalized read count data and identified significantly higher proportions of monocytes, erythroid cells, plasma cells, and innate lymphoid cells, as well as a significantly lower number of dendritic cells, in iMCD-TAFRO compared to sentinel controls (Figure 2A). Our data also suggest significantly more monocytes and innate lymphoid cells and significantly fewer dendritic cells in iMCD-IPL/NOS compared to controls (Figures 2B, C).

We identified potential treatment approaches that could be used in iMCD by examining both iMCD (all subtype) and iMCD-TAFRO gene signatures using the LINCS1000 database. DEGs with a log_2FC greater than |1.5| from each comparison were used

TABLE 3 Top 20 genes by log_2 fold change in the discovery iMCD-TAFRO cohort, with corresponding validation cohort statistics, adjusted p-values, and ranks in both cohorts.

Gene	log2FC (validation)	log2FC (discovery)	Adjusted p (validation)	Adjusted P (discovery)	Rank (validation)	Rank (discovery)
SPP1	7.62	5.99	3.50E-17	3.21E-03	1	1
PLA2G2A	3.10	5.04	2.15E-03	2.02E-03	15	2
UTY	4.21	4.92	2.46E-02	1.08E-02	11	3
LBP	6.37	4.81	6.08E-12	1.05E-07	2	4
MGAM	5.21	3.93	1.19E-12	8.79E-03	4	5
AQP9	4.93	3.93	1.72E-12	2.58E-02	7	6
POSTN	2.87	3.88	4.01E-07	8.53E-06	16	7
SLC19A2	2.54	3.82	1.10E-14	3.00E-01	18	8
INHBB	3.41	3.54	1.03E-10	2.17E-02	14	9
HLA-DQA2	5.04	3.52	4.50E-06	1.29E-01	5	10
STON1-GTF2A1L	2.34	3.51	2.65E-04	6.79E-02	19	11
IGKV3D-15	3.84	3.47	8.03E-07	6.08E-02	12	12
STS	4.73	3.43	3.04E-05	3.42E-01	9	13
PLPPR4	3.79	3.42	2.62E-14	4.23E-06	13	14
NUDCD1	5.33	3.27	1.88E-24	7.20E-02	3	15
IGLV2-18	1.46	3.24	2.85E-02	2.17E-01	20	16
S100A8	4.33	3.21	1.73E-11	7.61E-03	10	17
SERPINE1	2.76	3.20	4.21E-05	1.64E-04	17	18
RP11-561B11.2	4.74	3.07	7.43E-11	1.29E-01	8	19
HSPA5	4.98	3.05	1.35E-04	7.11E-02	6	20



C.

Cell Type	Mean sentinel control cell proportion	Mean iMCD-TAFRO cell proportion	Mean iMCD-NOS/iMCD-IPL cell proportion	iMCD-TAFRO vs Sentinel Control P-value	iMCD-NOS/iMCD-IPL vs Sentinel Control P-value	iMCD-TAFRO vs Sentinel Control adjusted P-value	iMCD-NOS/iMCD-IPL vs Sentinel Control adjusted P-value
B cells	31.1	26.9	28.2	5.90×10^{-5}	0.0103	7.67×10^{-4}	0.134
Cycling cells	2.66	1.53	2.04	0.489	0.876	1.00	1.00
DC	1.81	0.182	0.293	1.40×10^{-4}	0.00151	0.00182	0.0197
Erythroid	0.215	0.800	0.578	2.10×10^{-5}	0.00519	2.73×10^{-4}	0.0675
HSC/MPP	0.0309	0.0352	0.0156	0.449	1.00	1.00	1.00
ILC	1.48	4.92	4.47	5.71×10^{-6}	7.12×10^{-4}	7.42×10^{-5}	0.00926
Macrophages	0.331	0.177	0.155	0.487	0.550	1.00	1.00
Mast cells	0.428	0.133	0.0398	0.0399	0.0109	0.519	0.142
Monocytes	0.0542	0.585	0.213	1.97×10^{-7}	0.00143	2.57×10^{-6}	0.0186
Plasma cells	0.225	1.22	1.08	3.33×10^{-5}	0.0432	4.33×10^{-4}	0.562
Promyelocytes	0.0150	0.00784	0.0173	0.147	0.102	1.00	1.00
T cells	61.3	62.8	62.1	0.176	0.600	1.00	1.00
pDC	0.385	0.699	0.783	0.00245	0.0275	0.0318	0.357

FIGURE 2
Inferred cell type population changes in iMCD clinical subtypes and sentinel controls. Cell types predicted to be significantly up- or down-regulated in **(A)** iMCD-TAFRO vs. SLN or **(B)** iMCD-NOS/IPL vs SLN. **(C)** Shows all cell type proportion predictions. dendritic cells (DC), innate lymphoid cells (ILC), Plasmacytoid Dendritic Cells (pDCs).

to identify predicted reversing drug treatments (Figures 3A–F, Supplementary Tables 6-8). Interestingly, sirolimus, a known treatment in iMCD, emerged as a top choice for reversal of the iMCD (all subtype) and iMCD-TAFRO gene signatures (Figures 3A, B, D, Supplementary Table 7). When DEGs from the TAFRO subtype were considered, interesting new potential new drugs emerge such as the VEGF inhibitor, sorafenib (Figure 3C, Supplementary Table 8).

Orthogonal gene expression analysis of iMCD subtypes shows shared and unique gene signatures

To determine unique and shared gene signatures between iMCD clinical subtypes and clinicopathologically related disorders, we performed targeted transcriptomic analysis of 594 immune-related genes using an orthogonal targeted gene expression platform (Nanostring nCounter) on iMCD-TAFRO (n=12), iMCD-NOS (n=4), iMCD-IPL (n=3), sentinel controls (n=8), SLE (n=3), and DLBCL (n=5) (Table 1). We then compared the DEGs identified using this method with those from the discovery bulk RNA-seq analysis and found that, among the 468 overlapping genes, the direction of association and fold change were highly correlated between the two methods (Supplementary Figure 5).

As expected, some DEGs were upregulated in all iMCD subtypes; however, each clinical subtype also exhibited unique gene expression signatures. Four DEGs were significantly upregulated across all clinical subtypes (*SPP1*, *PRDM1*, *XBP1*, and *CLU*; Figure 4, Supplementary Table 11) and were also significantly upregulated in the bulk RNA-seq iMCD-TAFRO data. Notably, *CLU* was the only gene uniformly upregulated across the three iMCD clinical subtypes and was not significantly upregulated in either of the clinicopathologically related disorders.

10.3389/fimmu.2026.1872505

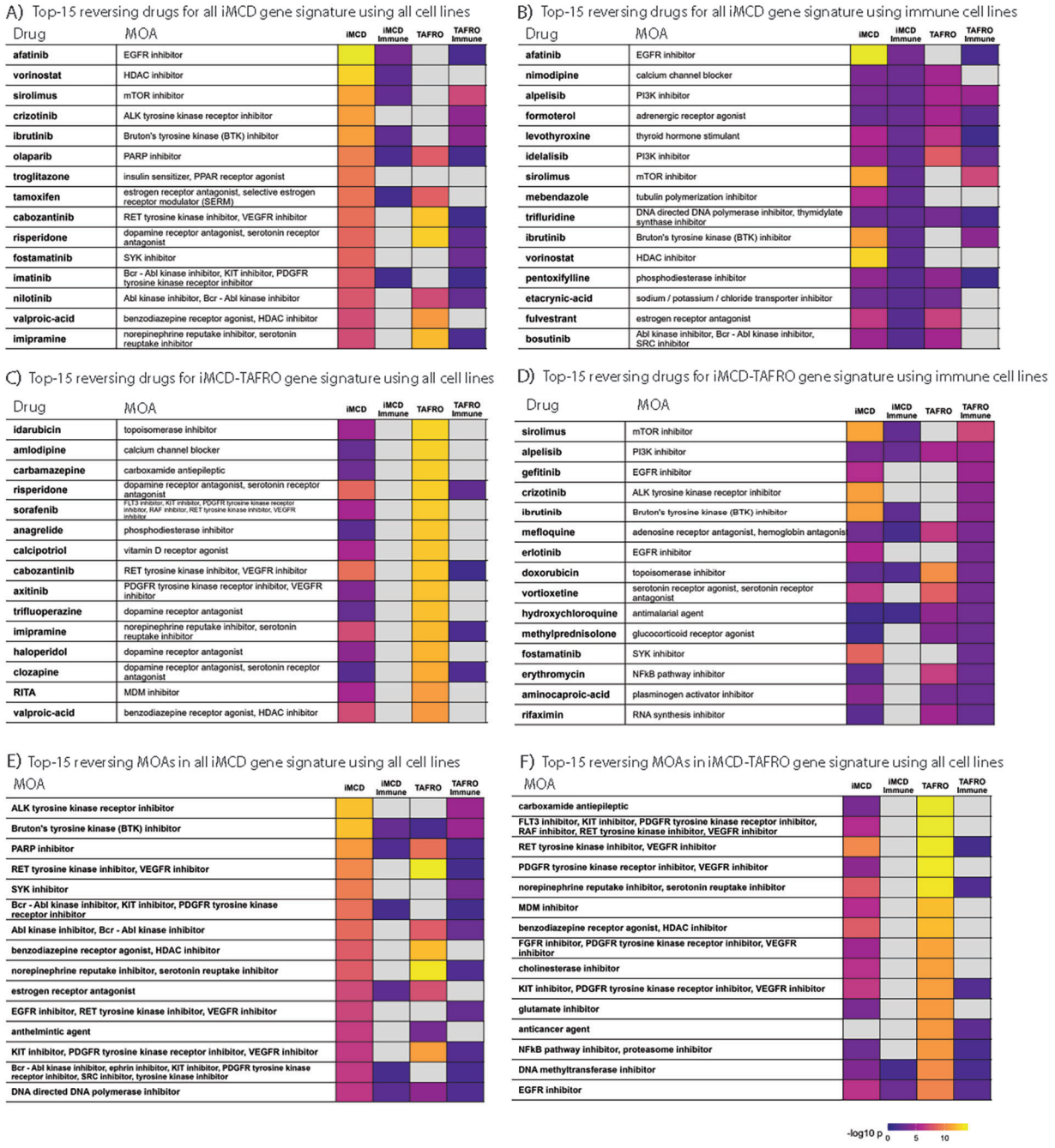


FIGURE 3

LINCS1000 identifies treatments predicted to reverse gene signatures in iMCD (all subtypes) and iMCD-TAFRO lymph node tissue. The heatmap encodes the LINCS1000 enrichment as –log10(p_global). Grey indicates that no cell lines were tested for that MOA or drug. Each row lists a Drug (bold) with its mechanism of action (MOA). **(A–D)** are scores for iMCD genes (all cell lines), iMCD genes (immune-restricted cell lines), TAFRO genes (all cell lines), and TAFRO genes (immune-restricted cell lines). **(A–D)** are sorted by these columns to display the top 15 for each. **(E, F)** aggregate drugs by MOA, displaying the top 15 MOAs ranked by median $-\log_{10}$(p_global) for iMCD and TAFRO gene signatures. 5-HT, serotonin; ACh, acetylcholine; AChE, acetylcholinesterase; act., activator; ag., agonist; aggr., aggregation; antag., antagonist; blk., blocker; COX, cyclooxygenase; DA, dopamine; DH, dehydrogenase; immunosupp., immunosuppressant; inh., inhibitor; mod., modulator; MTase, methyltransferase; NE, norepinephrine; PDE, phosphodiesterase; pol., polymerase; prod., production; rec., receptor; repl., replication; reup., reuptake; stim., stimulant; synth., synthesis; TK, tyrosine kinase; topo., topoisomerase; transp., transporter.

10.3389/fimmu.2026.1872505

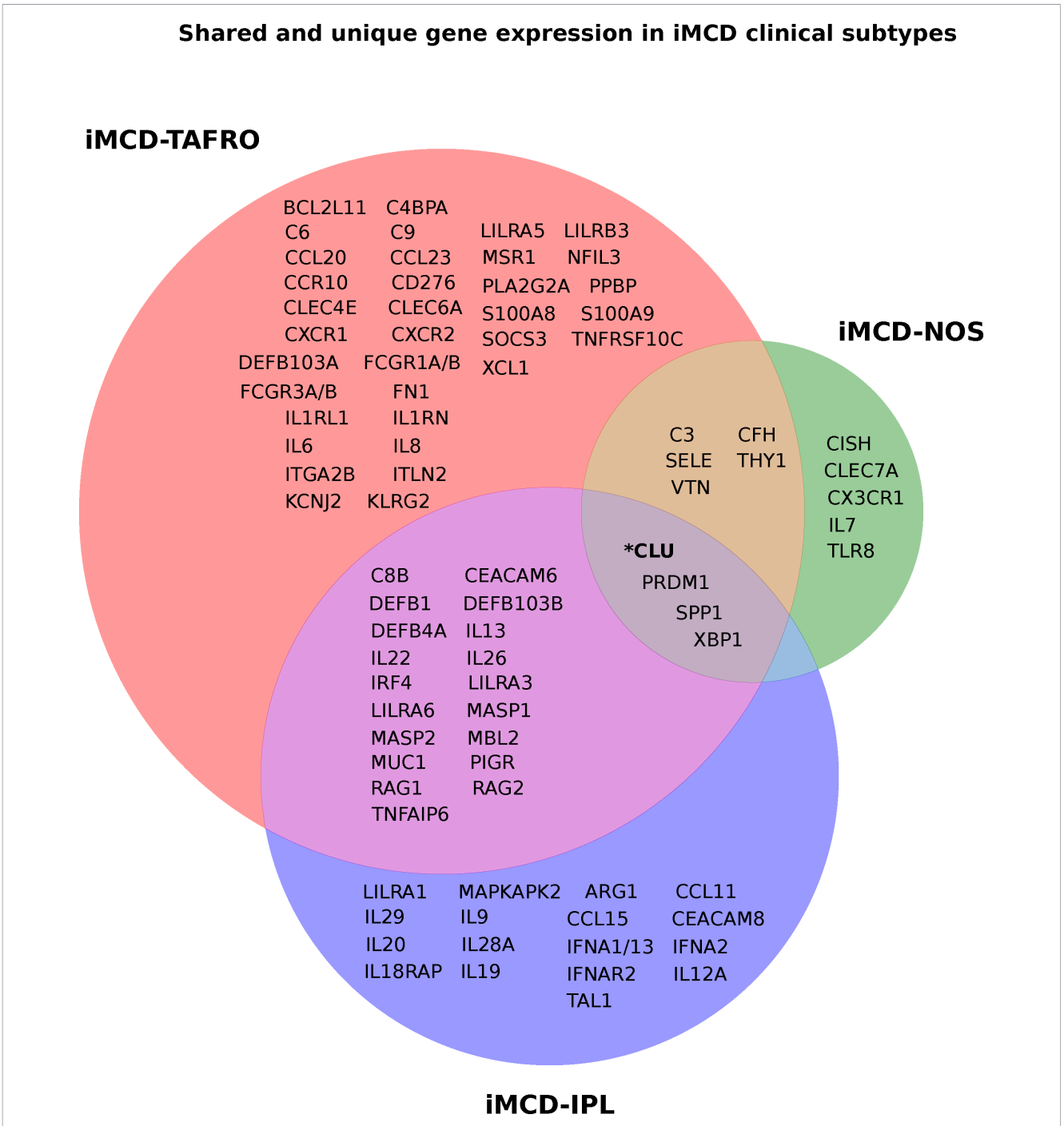


FIGURE 4
Shared and unique gene expression in iMCD clinical subtypes. Shared and unique genes in the targeted Nanostring gene expression panel in each iMCD clinical subtype. CLU was the only gene that was significantly upregulated in all 3 clinical subtypes, but not in any of the disease comparators.

There were also genes that exhibited subset-specific differential expression. There were 44 unique DEGs in iMCD-TAFRO (35 upregulated, 9 downregulated), 45 unique DEGs in iMCD-IPL (17 upregulated, 28 downregulated), and 12 unique DEGs in iMCD-NOS (5 upregulated, 7 downregulated (Figure 4, Supplementary Tables 11-13). The top unique DEGs in iMCD-TAFRO were *PLA2G2A*, *MSR1*, and *IL8*, in MCD-IPL were *IL9*, *KIR3DL1*, and *IL18RAP*, and in iMCD-NOS were *IL7*, *TLR8*, and *CX3CR1* (Supplementary Tables 11-13).

Clusterin expression in regions of iMCD LN tissue and germinal center features differentiate iMCD from select lymphadenopathies

CLU was the only gene uniformly upregulated in iMCD clinical subtypes but not in any disease comparator groups. Furthermore, it is known as a marker for follicular dendritic cells (FDCs), a fibroblastic lymph node stromal cell known whose histologic

10.3389/fimmu.2026.1872505

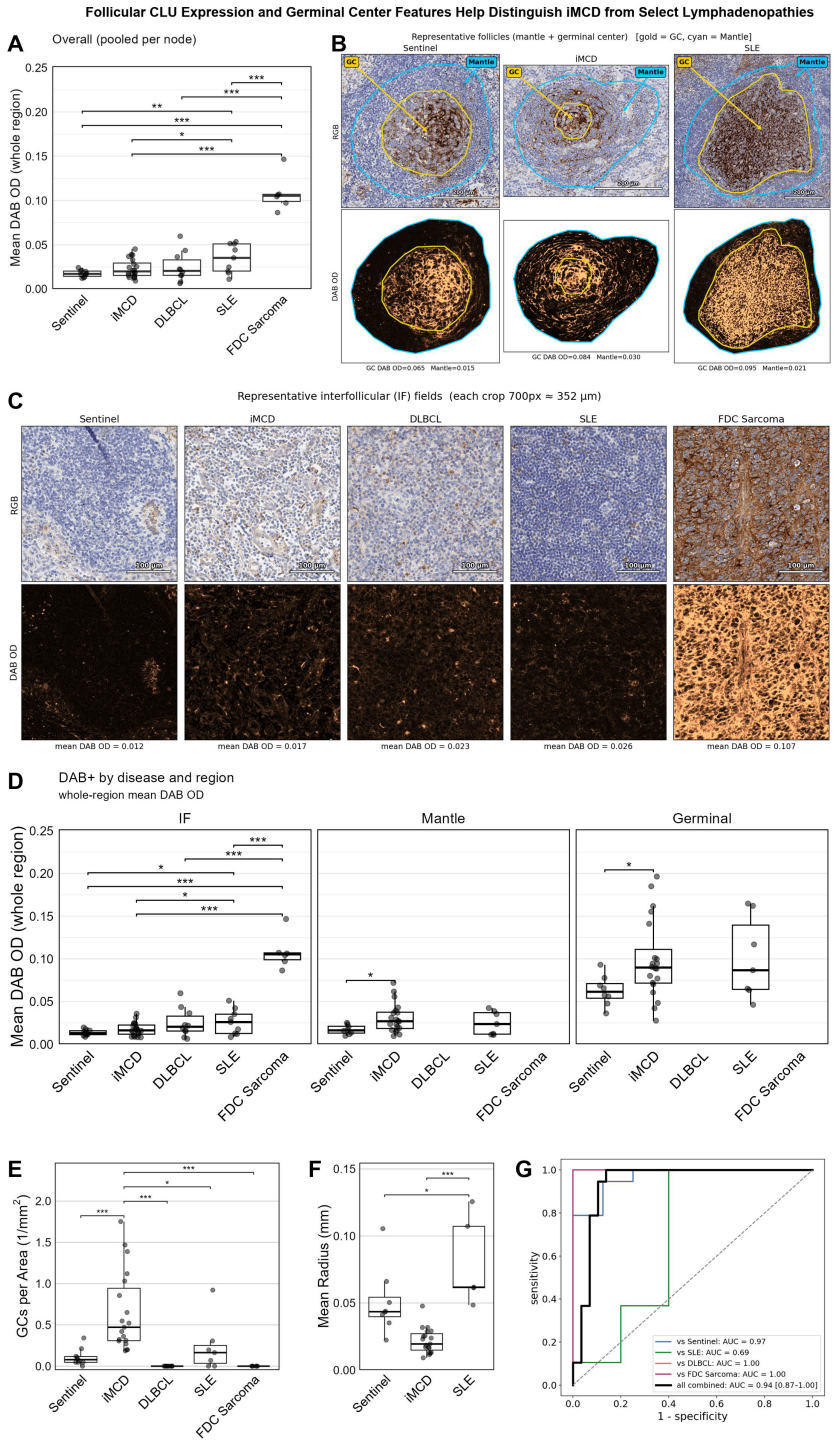


FIGURE 5

Follicular CLU expression and germinal center features help distinguish iMCD from select lymphadenopathies. Lymph nodes from sentinel (control), iMCD, DLBCL, SLE, and FDC Sarcoma patients were immunohistochemically stained for Clusterin protein using DAB and hematoxylin and imaged at 20X. Clusterin abundance was quantified as the mean DAB optical density (OD) within each region, computed from the color-deconvolved DAB channel. **(A)** Mean DAB OD across the whole lymph node region, pooled per node, for all conditions. **(B)** Representative follicles for sentinel, iMCD, and SLE lymph nodes, shown as RGB (top) and DAB OD (bottom), with the germinal center (gold) and mantle zone (cyan) outlined; mean DAB OD values for the GC and mantle are indicated. **(C)** Representative interfollicular (IF) fields for each condition, shown as the RGB image (top) and the corresponding DAB OD map (bottom); the mean DAB OD of each field is indicated below (each field ≈ 352 µm; scale bars, 100 µm). **(D)** Mean DAB OD by region (IF, mantle zone, and germinal center) for each condition. DLBCL and FDC Sarcoma had no identifiable germinal centers or mantle zones, and some sentinel lymph nodes had very few identifiable germinal centers. **(E)** The number of germinal centers per lymph node area (per mm^2). **(F)** The mean radius of quantified germinal centers in each condition. **(G)** ROC analysis discriminating iMCD from non-Castleman lymphadenopathy. Coloured curves, the combined model's separation of iMCD from each comparator (vs sentinel, AUC 0.97; vs SLE, 0.69; vs DLBCL and vs FDC sarcoma, both 1.00); black curve, the full combined model (compartment-resolved CLU intensity, GC density, GC size; AUC 0.94, 95% CI 0.87–1.00). **(A, D, E, F)** Statistical significance: ANOVA + Tukey test. P-value: *** <.001, ** <.01, * <.05.

prominence is a defining pathologic feature of Castleman. Markers such as CR1, CR2, FCER2, LTBR, FDCSP, and VCAM1 can help identify expanded follicular dendritic cell networks in Castleman disease. Importantly, CLU expression showed only modest and variable correlation with these FDC-associated genes, with stronger correlation for select markers such as FDCSP and VCAM1 but weak or absent correlation with canonical markers, including CR1, CR2, FCER2, and LTBR (Supplementary Table 14). These findings suggest that CLU expression may not simply reflect broad FDC enrichment. However, further studies will be required to determine whether CLU provides additive diagnostic or biological information beyond established FDC-associated markers and whether it represents a disease-specific biomarker in iMCD.

We therefore asked if *CLU* could distinguish iMCD from related diseases by single-plex immunohistochemistry, a widely used tool in pathologic diagnosis. We performed immunohistochemistry using the Clusterin protein, which is recognized by a robust and reproducible IHC. We quantified the area of positive Clusterin staining out of the total LN area in iMCD (n=20), two overlapping conditions (DLBCL, n=10, SLE, n=10), a condition known to have increased Clusterin (FDC sarcoma, n=6), and sentinel controls (n=10). As expected, FDC sarcoma had significantly increased Clusterin staining across the entire LN (Figure 5A). Next, we evaluated whether there were differences in Clusterin staining in different regions of the LN between disease groups. iMCD was the only disease group with significantly increased Clusterin staining in the MZ and the GC compared to sentinel LNs (Figures 5B, D). However, in the IF space, FDC sarcoma showed the most significant increase in Clusterin staining (Figures 5C, D). While the mean Clusterin DAB OD per GC was likely not striking enough to explain the increased clusterin observed globally in the LN-wide transcriptomic analysis, we found that there were significantly more GCs per area of the LN compared to related diseases and controls (Figure 5E), despite a significantly smaller size (Figure 5F). A model integrating regional Clusterin intensity with germinal-center density and size separated iMCD from non-iMCD LNs with an overall AUC of 0.94 (95% CI 0.87–1.00; permutation P = 0.001; Figure 5G). Discrimination was perfect against the lymphomas (DLBCL, FDC sarcoma; AUC 1.00) and high against sentinel reactive controls (0.97), but limited against SLE (0.69). Together, these analyses show that Clusterin is elevated in the GCs and MZs of iMCD patient LNs, and that these regions are more numerous in iMCD patient LNs than in related diseases.

Discussion

This study is the first to employ multiple transcriptomic techniques across distinct subtypes of iMCD and various disease-control groups to characterize the LN transcriptome of these subtypes. We identified enrichment of several genes and gene networks previously described and consistent with disease biology, such as angiogenesis, cell proliferation, and various aspects of the immune response, including the IL-6-JAK-STAT pathway and mTORC1 signaling, which we previously discovered. Identifying these known pathways provides confidence in the ability to discover novel biologically plausible mechanisms. In addition to IL-6, several genes within the IL-6-JAK-STAT network were significantly up-regulated (*SOCS3, OSMR, PIM1*). Even though the IL-6-JAK-STAT pathway is enriched in the serum of both IL-6-responsive and IL-6-refractory patients, IL-6 blockade is effective in approximately 35-50% of patients (4), prompting investigation into alternative mechanisms for IL-6-JAK-STAT activation in the absence of IL-6 (3). Recently, JAK inhibitors have been shown to be effective in alleviating symptoms in a subset of IL-6-refractory patients (34, 35).

After successfully validating a substantial number of upregulated genes and pathways identified in a discovery cohort of iMCD-TAFRO patients, we performed a targeted transcriptomic comparison between the differing iMCD subgroups using an orthogonal targeted gene expression assay. When looking for genes highly upregulated in each of the subtypes, we identified *SPP1*, *PRDM1*, *XBP1*, and *CLU*. *CLU* was the only gene that was upregulated in each iMCD clinical subtype, but not in any other disease group. Osteopontin (*SPP1*) regulates the inflammatory response and enhances the expression of VEGF family growth factor (36, 37). It was also found to be upregulated in a previous transcriptome-based study in MCD LN tissue, although clinical subset-level data were not available (13). Interestingly, one of the top therapeutic 'reversers' predicted from the enriched gene set signature in iMCD-TAFRO LN tissue was the VEGF inhibitor sorafenib, which, given these findings and the clinical observations of hypervascularization, warrants further investigation.

The upregulation of CLU across each subgroup was also interesting, as it serves as a follicular dendritic cell marker and mediates the clearance of apoptotic cells, thereby potentially preventing an apoptotic cell-induced autoimmune response (38). Because iMCD GCs undergo high GC B-cell turnover, CLU may be upregulated to facilitate debris clearance (39). High Clusterin levels could also inhibit dendritic cell death, increasing T-cell priming (40). FDCs internalize, recycle, and re-display complement-coated immune complexes via CR1 and CR2, presenting antigen to B-cells (41). Antigen presentation is a key driver in GC persistence and prolonged immune response (42). Clusterin binds terminal complement components and circulating immune complexes, forming soluble, non-lytic C5b-9, which could stabilize immune complexes in complement-rich follicles (41). Together, this suggests that *CLU* may play a role in GC persistence, B-cell activation, and plasma cell differentiation. Interestingly, *PRDM1* and *XBP1* are both transcription factors essential for the terminal differentiation of B cells into antibody-secreting plasma cells, suggesting a potential role for GC dysfunction in plasma cell differentiation.

In addition to differences in CLU expression between the GC and MZs of iMCD patients, we also observed significant differences in GC frequency and size compared with those in specific related disease controls. Taken together, this may suggest that the significant global increase in CLU expression observed in bulk transcriptomics is related to modestly increased CLU expression per unit area in the GC and MZ, as well as to substantially more GCs per

unit area. Importantly, individual mantle zones and germinal centers were identified histologically, allowing CLU expression to be quantified within defined lymph node compartments. This compartment-level analysis demonstrated increased CLU expression in both mantle zones and germinal centers from iMCD lymph nodes compared with sentinel lymph nodes, suggesting that increased CLU expression is not explained solely by increased germinal center abundance. However, because CLU expression and germinal center abundance were assessed in the same histologic specimens, the current study cannot determine whether increased CLU expression contributes to germinal center expansion or represents a correlated feature of the iMCD lymph node microenvironment. A composite model incorporating CLU expression in the germinal center and mantle zone, GC density, and GC size demonstrated strong discriminatory performance for differentiating iMCD from selected related diseases (AUC 0.94), although validation in larger, independent cohorts will be needed to determine its broader diagnostic utility.

This study has several limitations. First, the cohort sizes are small, especially in the targeted gene expression cohort, reflecting the rarity of iMCD and the limited availability of well-characterized lymph node tissue from affected patients. The subtype-specific differences in gene expression should be interpreted in light of the limited sample size, as the number of iMCD-IPL (n=3) and iMCD-NOS (n=4) samples was small. Accordingly, these subtype-associated signatures should be viewed as exploratory observations that require validation in larger, independent cohorts. Second, cell-type deconvolution was performed using reference data derived from healthy donor lymph nodes. Given the architectural histology and immune activation characteristic of iMCD lymph nodes, this reference dataset may not fully capture disease-associated cellular states, which should be considered when interpreting inferred changes in plasma cells, monocytes, innate lymphoid cells, and other immune populations. Third, comparator groups included in this study were limited and do not encompass the full spectrum of lymphadenopathies that may enter the differential diagnosis of iMCD. Additional mimics, including IgG4-related disease, Rosai-Dorfman disease, angioimmunoblastic T-cell lymphoma, reactive follicular hyperplasia, HHV-8-associated MCD, and other autoimmune or inflammatory lymphadenopathies, were not included. Therefore, the ability of CLU expression to distinguish iMCD should be interpreted within the context of the comparator groups analyzed here. Larger validation studies, including a broader range of diagnostic mimics, will be needed to establish the broader specificity of CLU expression in iMCD. Finally, the LINCS-based drug repurposing analysis is entirely computational and should be considered hypothesis-generating. Although this approach identified biologically plausible candidates, including sirolimus, the predicted therapeutic relevance of these agents requires experimental and clinical validation before firm conclusions can be drawn.

In summary, we have conducted a comprehensive transcriptome investigation of iMCD LN tissue, with a particular focus on iMCD-TAFRO, the most severe subtype of iMCD. To extend those observations, we also used a targeted gene expression panel of immunology and inflammation-related genes in an expanded cohort of iMCD subtypes and other inflammatory disorders to identify shared and unique gene expression signatures in iMCD. Our findings support and validate previously identified gene markers in 'omics-level investigations in multiple tissues in iMCD and provide additional functional candidates for further investigation. In addition, a composite model incorporating CLU expression in the germinal center and mantle zone, GC density, and GC size showed strong discriminatory performance for differentiating iMCD from selected related lymphadenopathies, supporting the potential value of integrating molecular and histomorphometric features. Together, these findings illuminate unique pathological mechanisms at play in iMCD lymph node tissue and provide a framework for future diagnostic and mechanistic studies.

Data availability statement

All Nanostring nCounter gene expression and bulk RNA sequencing data in this manuscript are available at GEO under the following GSE accession numbers: Nanostring nCounter: GSE336631 and bulk RNAseq: GSE337015. Publicly available data used in this paper can be found under the following GSE accession: GSE195477.

Ethics statement

The studies involving humans were approved by the Institutional Review Board of the University of Pennsylvania (IRB # 824758). The studies were conducted in accordance with the local legislation and institutional requirements. The participants provided their written informed consent to participate in this study.

Author contributions

MG: Conceptualization, Data curation, Formal analysis, Investigation, Methodology, Project administration, Software, Supervision, Validation, Visualization, Writing – original draft, Writing – review & editing. KW: Data curation, Formal analysis, Investigation, Methodology, Software, Validation, Visualization, Writing – original draft, Writing – review & editing. JZ: Conceptualization, Formal analysis, Investigation, Methodology, Validation, Visualization, Writing – original draft, Writing – review & editing. MM: Conceptualization, Formal analysis, Investigation, Project administration, Validation, Visualization, Writing – original draft, Writing – review & editing. KF: Data curation, Formal analysis, Investigation, Methodology, Validation, Writing – original draft, Writing – review & editing. AI: Data curation, Formal analysis, Investigation, Methodology, Validation,

Writing – original draft, Writing – review & editing. JB: Conceptualization, Investigation, Methodology, Project administration, Writing – original draft, Writing – review & editing. SG: Formal analysis, Investigation, Methodology, Writing – original draft, Writing – review & editing. LZ: Investigation, Methodology, Project administration, Writing – original draft, Writing – review & editing. SP: Project administration, Writing – original draft, Writing – review & editing, Conceptualization, Investigation, Methodology. BA: Investigation, Methodology, Project administration, Resources, Validation, Writing – original draft, Writing – review & editing. DF: Conceptualization, Investigation, Methodology, Project administration, Resources, Supervision, Validation, Writing – original draft, Writing – review & editing.

Funding

The author(s) declared that financial support was received for this work and/or its publication. This work was supported by the National Heart, Lung, and Blood Institute (R01HL141408), US Food & Drug Administration (R01FD007632), the Colton Center for Autoimmunity at the University of Pennsylvania, the Orphan Disease Center at the University of Pennsylvania, and the Castleman Disease Collaborative Network.

Acknowledgments

The authors wish to thank Pedro Horna as well as scientists at Tempus Biosciences and the Wistar Institute for their analytical contributions and guidance. The authors also wish to thank Marjorie Raines, Elana Amsterdam (Elana Amsterdam Health and Wellness Fund), Paul Robbins, Peter Taylor, and Maria-Elena Cobena for their support of this work.

Conflict of interest

The author(s) declared that this work was conducted in the absence of any commercial or financial relationships that could be construed as a potential conflict of interest.

Generative AI statement

The author(s) declared that generative AI was not used in the creation of this manuscript.

Any alternative text (alt text) provided alongside figures in this article has been generated by Frontiers with the support of artificial intelligence and reasonable efforts have been made to ensure accuracy, including review by the authors wherever possible. If you identify any issues, please contact us.

Publisher's note

All claims expressed in this article are solely those of the authors and do not necessarily represent those of their affiliated organizations, or those of the publisher, the editors and the reviewers. Any product that may be evaluated in this article, or claim that may be made by its manufacturer, is not guaranteed or endorsed by the publisher.

Supplementary material

The Supplementary Material for this article can be found online at: https://www.frontiersin.org/articles/10.3389/fimmu.2026.1872505/full#supplementary-material

References

1. Munshi N, Mehra M, van de Velde H, Desai A, Potluri R, Vermeulen J. Use of a claims database to characterize and estimate the incidence rate for Castleman disease. *Leuk Lymphoma*. (2015) 56:1252–60. doi: 10.3109/10428194.2014.953145

2. Dispenzieri A, Armitage JO, Loe MJ, Geyer SM, Allred J, Camoriano JK, et al. The clinical spectrum of Castleman's disease. *Am J Hematol*. (2012) 87:997–1002. doi: 10.1002/ajh.23291

3. Pierson SK, Shenoy S, Oromendia AB, Gorzewski AM, Langan Pai R, Nabel CS, et al. Discovery and validation of a novel subgroup and therapeutic target in idiopathic multicentric Castleman disease. *Blood Adv*. (2021) 5:3445–56. doi: 10.1182/bloodadvances.2020004016

4. van Rhee F, Voorhees P, Dispenzieri A, Fosså A, Srkalovic G, Ide M, et al. International, evidence-based consensus treatment guidelines for idiopathic multicentric Castleman disease. *Blood*. (2018) 132:2115–24. doi: 10.1182/blood-2018-07-862334

5. Fajgenbaum DC. Novel insights and therapeutic approaches in idiopathic multicentric Castleman disease. *Hematol Am Soc Hematol Educ Program*. (2018) 2018:318–25. doi: 10.1182/blood-2018-05-848671

6. Fajgenbaum DC, Wu D, Goodman A, Wong R, Chadburn A, Nasta S, et al. Insufficient evidence exists to use histopathologic subtype to guide treatment of idiopathic multicentric Castleman disease. *Am J Hematol*. (2020) 95:1553–61. doi: 10.1002/ajh.25992

7. van Rhee F, Wong RS, Munshi N, Rossi J-F, Ke X-Y, Fosså A, et al. Siltuximab for multicentric Castleman's disease: a randomised, double-blind, placebo-controlled trial. *Lancet Oncol*. (2014) 15:966–74. doi: 10.1016/s1470-2045(14)70319-5

8. Pierson SK, Katz L, Nabel CS, Ruth JR, Diamond S, Karvir H, et al. Quantitative changes in serum proteins including CXCL13 are early indicators of response to anti-IL6 therapy in idiopathic multicentric Castleman disease. *Blood*. (2019) 134:3599. doi: 10.1182/blood-2019-128284

9. Pierson SK, Katz L, Williams R, Mumau M, Gonzalez M, Guzman S, et al. CXCL13 is a predictive biomarker in idiopathic multicentric Castleman disease. *Nat Commun*. (2022) 13:7236. doi: 10.1038/s41467-022-34873-7

10. Pai R-AL, Japp AS, Gonzalez M, Rasheed RF, Okumura M, Arenas D, et al. Type I IFN response associated with mTOR activation in the TAFRO subtype of idiopathic multicentric Castleman disease. *JCI Insight*. (2020) 5:e135031. doi: 10.1172/jci.insight.135031

11. Pierson SK, Stonestrom AJ, Shilling D, Ruth J, Nabel CS, Singh A, et al. Plasma proteomics identifies a "chemokine storm" in idiopathic multicentric Castleman disease. *Am J Hematol*. (2018) 93:902–12. doi: 10.1002/ajh.25123

12. Wing A, Xu J, Meng W, Rosenfeld AM, Li EY, Wertheim G, et al. Transcriptome and unique cytokine microenvironment of Castleman disease. *Mod Pathol*. (2022) 35:451–61. doi: 10.1038/s41379-021-00950-3

13. Horna P, King RL, Jevremovic D, Fajgenbaum DC, Dispenzieri A. The lymph node transcriptome of unicentric and idiopathic multicentric Castleman disease. *Haematologica*. (2022) 108(1):207–18. doi: 10.3324/haematol.2021.280370

14. Nishikori A, Nishimura MF, Nishimura Y, Otsuka F, Maehama K, Ohsawa K, et al. Idiopathic plasmacytic lymphadenopathy forms an independent subtype of idiopathic multicentric castleman disease. *Int J Mol Sci*. (2022) 23:10301. doi: 10.3390/ijms231810301

15. Oksenhendler E, Boutboul D, Fajgenbaum D, Mirouse A, Fieschi C, Malphettes M, et al. The full spectrum of Castleman disease: 273 patients studied over 20 years. *Br J Haematol*. (2018) 180:206–16. doi: 10.1111/bjh.15019

16. Fajgenbaum DC, Uldrick TS, Bagg A, Frank D, Wu D, Srkalovic G, et al. International, evidence-based consensus diagnostic criteria for HHV-8-negative/idiopathic multicentric Castleman disease. *Blood*. (2017) 129:1646–57. doi: 10.1182/blood-2016-10-746933

17. Iwaki N, Fajgenbaum DC, Nabel CS, Gion Y, Kondo E, Kawano M, et al. Clinicopathologic analysis of TAFRO syndrome demonstrates a distinct subtype of HHV-8-negative multicentric Castleman disease: Clinicopathologic Analysis of TAFRO Syndrome. *Am J Hematol*. (2016) 91:220–6. doi: 10.1002/ajh.24242

18. Gao Y-H, Liu Y-T, Zhang M-Y, Li S-Y, Fajgenbaum DC, Zhang L, et al. Idiopathic multicentric Castleman disease (iMCD)-idiopathic plasmacytic lymphadenopathy: A distinct subtype of iMCD-not otherwise specified with different clinical features and better survival. *Br J Haematol*. (2024) 204:1830–7. doi: 10.1111/bjh.19334

19. Michuda J, Breschi A, Kapilivsky J, Manghnani K, McCarter C, Hockenberry AJ, et al. Validation of a transcriptome-based assay for classifying cancers of unknown primary origin. *Mol Diagn Ther*. (2023) 27:499–511. doi: 10.1007/s40291-023-00650-5

20. Bray NL, Pimentel H, Melsted P, Pachter L. Near-optimal probabilistic RNA-seq quantification. *Nat Biotechnol*. (2016) 34:525–7. doi: 10.1038/nbt.3519

21. Lawrence M, Huber W, Pagès H, Aboyoun P, Carlson M, Gentleman R, et al. Software for computing and annotating genomic ranges. *PloS Comput Biol*. (2013) 9: e1003118. doi: 10.1371/journal.pcbi.1003118

22. Love MI, Huber W, Anders S. Moderated estimation of fold change and dispersion for RNA-seq data with DESeq2. *Genome Biol*. (2014) 15:550. doi: 10.1186/s13059-014-0550-8

23. Subramanian A, Tamayo P, Mootha VK, Mukherjee S, Ebert BL, Gillette MA, et al. Gene set enrichment analysis: a knowledge-based approach for interpreting genome-wide expression profiles. *Proc Natl Acad Sci USA*. (2005) 102:15545–50. doi: 10.1073/pnas.0506580102

24. Liberzon A, Birger C, Thorvaldsdóttir H, Ghandi M, Mesirov JP, Tamayo P. The Molecular Signatures Database (MSigDB) hallmark gene set collection. *Cell Syst*. (2015) 1:417–25. doi: 10.1016/j.cels.2015.12.004

25. Ritchie ME, Phipson B, Wu D, Hu Y, Law CW, Shi W, et al. limma powers differential expression analyses for RNA-sequencing and microarray studies. *Nucleic Acids Res*. (2015) 43:e47. doi: 10.1093/nar/gkv007

26. Nickles D, Sandmann T, Ziman R, Bourgon R. *NanoStringQCPro: Quality metrics and data processing methods for NanoString mRNA gene expression data*. Boston, MA, USA: Bioconductor (2022).

27. Bhattacharya A, Hamilton AM, Furberg H, Pietzak E, Purdue MP, Troester MA, et al. An approach for normalization and quality control for NanoString RNA expression data. *Brief Bioinform*. (2021) 22:1–13. doi: 10.1093/bib/bbaa163

28. Risso D, Ngai J, Speed TP, Dudoit S. Normalization of RNA-seq data using factor analysis of control genes or samples. *Nat Biotechnol*. (2014) 32:896–902. doi: 10.1038/nbt.2931

29. Domínguez Conde C, Xu C, Jarvis LB, Rainbow DB, Wells SB, Gomes T, et al. Cross-tissue immune cell analysis reveals tissue-specific features in humans. *Science*. (2022) 376:eabl5197. doi: 10.1126/science.abl5197

30. Jew B, Alvarez M, Rahmani E, Miao Z, Ko A, Garske KM, et al. Accurate estimation of cell composition in bulk expression through robust integration of single-cell information. *Nat Commun*. (2020) 11:1971. doi: 10.1038/s41467-020-15816-6

31. Marino GB, Evangelista JE, Clarke DJB , Ma'ayan A. L2S2: chemical perturbation and CRISPR KO LINCS L1000 signature search engine. *Nucleic Acids Res*. (2025) 53 (W1):W338–50. doi: 10.1093/nar/gkaf373

32. Subramanian A, Narayan R, Corsello SM, Peck DD, Natoli TE, Lu X, et al. A next generation Connectivity Map: L1000 platform and the first 1,000,000 profiles. *Cell*. (2017) 171:1437–1452.e17. doi: 10.1016/j.cell.2017.10.049

33. Risueño A, Hagner PR, Towfic F, Fontanillo C, Djebbari A, Parker JS, et al. Leveraging gene expression subgroups to classify DLBCL patients and select for clinical benefit from a novel agent. *Blood*. (2020) 135:1008–18. doi: 10.1182/blood.2019002414

34. Chen LYC, Skinnider BF, Wilson D, Fajgenbaum DC. Adrenalitis and anasarca in idiopathic multicentric Castleman's disease. *Lancet*. (2021) 397:1749. doi: 10.1016/s0140-6736(21)00674-7

35. Lust H, Gong S, Remiker A, Rossoff J. Idiopathic multicentric Castleman disease with TAFRO clinical subtype responsive to IL-6/JAK inhibition: A pediatric case series. *Pediatr Blood Cancer*. (2021) 68:e29261. doi: 10.1002/pbc.29261

36. Scatena M, Liaw L, Giachelli CM. Osteopontin: a multifunctional molecule regulating chronic inflammation and vascular disease. *Arterioscler Thromb Vasc Biol*. (2007) 27:2302–9. doi: 10.1161/ATVBAHA.107.144824

37. Wei T, Bi G, Bian Y, Ruan S, Yuan G, Xie H, et al. The significance of secreted phosphoprotein 1 in multiple human cancers. *Front Mol Biosci*. (2020) 7:565383. doi: 10.3389/fmolb.2020.565383

38. Cunin P, Beauvillain C, Miot C, Augusto J-F, Preisser L, Blanchard S, et al. Clusterin facilitates apoptotic cell clearance and prevents apoptotic cell-induced autoimmune responses. *Cell Death Dis*. (2016) 7:e2215. doi: 10.1038/cddis.2016.113

39. Wyatt AR, Yerbury JJ, Berghofer P, Greguric I, Katsifis A, Dobson CM, et al. Clusterin facilitates *in vivo* clearance of extracellular misfolded proteins. *Cell Mol Life Sci*. (2011) 68:3919–31. doi: 10.1007/s00018-011-0684-8

40. López Malizia A, Merlotti A, Bonte P-E, Sager M, Arribas De Sandoval Y, Goudot C, et al. Clusterin protects mature dendritic cells from reactive oxygen species mediated cell death. *Oncoimmunology*. (2024) 13:2294564. doi: 10.1080/2162402x.2023.2294564

41. Heesters BA, Chatterjee P, Kim Y-A, Gonzalez SF, Kuligowski MP, Kirchhausen T, et al. Endocytosis and recycling of immune complexes by follicular dendritic cells enhances B cell antigen binding and activation. *Immunity*. (2013) 38:1164–75. doi: 10.1016/j.immuni.2013.02.023

42. Matz HC, McIntire KM, Ellebedy AH. Persistent germinal center responses: slow-growing trees bear the best fruits. *Curr Opin Immunol*. (2023) 83:102332. doi: 10.1016/j.coi.2023.102332